EUROPEAN JOURNAL OF ENVIRONMENTAL AND CIVIL ENGINEERING, 2017
https://doi.org/10.1080/19648189.2017.1364299

Taylor & Francis
Taylor & Francis Group

Temporal and spatial distribution of the grout pressure and its effects on lining segments during synchronous grouting in shield tunnelling

Y. Liang[a], J. Zhang[b], Z. S. Lai[c], Q. Y. Huang[d] and L. C. Huang[a]

[a]School of Engineering, Sun Yat-Sen University, Guangzhou, China; [b]College of Civil and Transportation Engineering, Hohai University, Nanjing, China; [c]Glenn Department of Civil Engineering, Clemson University, Clemson, SC, USA; [d]School of Civil Engineering, Central South University, Changsha, China

ABSTRACT

The advance of tunnel shield creates void between the lining segments and the surrounding rock at the tail part of the tunnel shield. Grout is continuously injected into that void, to control the ground subsidence and maintain the segments stability. The grouting process must be precisely controlled and monitored to prevent any undesired significant subsidence or segment damage. In this work, a novel model to characterise the temporal and spatial distribution of the grout pressure in the rock-segment void is proposed, based on the theory of group diffusion and consolidation. The temporal variation of the grout viscosity is also considered in the proposed model. The proposed model is verified against field monitored data of the grout pressure, and exhibits quite good performance. Then a three-dimensional finite element model of the lining segments is developed to study the effects of the grout pressure on the mechanical response of the lining segments. The mechanical responses of the lining segments, in terms of internal force, moment and stress profile, are thoroughly analysed. These mechanical responses are also verified against the field monitored data, to further validate the proposed model of grout pressure distribution.

ARTICLE HISTORY
Received 13 April 2017
Accepted 29 July 2017

KEYWORDS
Shield tunnel; synchronous grouting; grout pressure distribution; varying grout viscosity; mechanical response of lining segments

1. Introduction

Benefiting from its superiorities in various aspects, shield tunnelling method is widely adopted in the construction of deep buried underground or underwater tunnels. With the advance of the tunnel shield, a void between the lining segments and the surrounding rock at the tail part of the tunnel shield (rock-segment void) is created, after the segments are pushed out of the shield tail. In order to control the ground subsidence and maintain the segments stability, the grout is required to be synchronously and continuously injected into that rock-segment gap. The grouting process must be precisely controlled and monitored. Any inappropriate settings in the grouting process, i.e. the injecting pressure or the injecting locations, would increase the risk of segments instability, such as dislocation, cracking, crushing and many others (Lin, Yang, Shang, & Xie, 2008; Liu & Yuan, 2015; Mo & Chen, 2008). The design of the grouting process brings up the following fundamental questions, what is the grout pressure distribution along the circumferential and longitudinal directions around the lining segments,

CONTACT L. C. Huang hlinch@mail.sysu.edu.cn

how is the grout pressure evolving with time, and how is the grout pressure affecting the mechanical response of the lining segments?

In the recent two decades, there have been a few attempts to address the aforementioned questions, from experimental, analytical and numerical perspectives. The field monitored data indicate that, there is notable increase in the internal force in the lining segments due to the grouting process, and the grout pressure decreases as the tunnel shield moving forward (Hashimoto, Nagaya, Konda, & Tamura, 2002; Liang, Su, & Fang, 2014; Tang, Chen, & Chen, 2009). As time elapses, the grout consolidates and grout pressure dissipates, resulting in a decrease in the internal force in the lining segments (Bezuijen, Talmon, Kaalberg, & Plugge, 2004; Talmon & Bezuijen, 2009). Numerical simulations, as well as analytical evaluations from (Do, Dias, & Oreste, 2014; Huang, Xu, & Zhou, 2009; Kasper & Meschke, 2006; Talmon & Bezuijen, 2013; Ye, Chen, & Jia, 2016) also give evidence that the grouting process has significant impact on the magnitude and distribution of the internal force in the lining segments. Thus, the grout pressure distribution becomes one of the key factors that impact the mechanical response of the lining segments.

It is worth noting that, when characterising the grout pressure distribution, the aforementioned researches only considered the diffusion process of the grout (the flow of grout), and did not take into the consideration of the consolidation process. In fact, as the grout being injected into the rock-segment void, the diffusion process of the grout is accompanied by the process of grout dewatering and consolidation under the confining effect from the surrounding rock. During the consolidation process of grout, the grout pressure dissipates as the cement and water seeping out from the grout aggregates and permeating into the surrounding rock. Recently, Zhang (2012) and Bai (2011) proposed to use grout consolidation and pressure dissipation theory to characterise the grout pressure distribution, based on the observations from laboratory experiments. But the temporal variation of the grout viscosity is not considered in his work. Researches (Bezuijen & Talmon, 2006; Han, Zhong, & Yu, 2007; Youn & Breitenbücher, 2014) indicate that the viscosity of the cement-based grout used in synchronously grouting process is increasing with time. And Ruan (2005) suggested that the grout viscosity had crucial impact on grouting pressure distribution. Therefore, to more accurately characterise the grout distribution, the diffusion and consolidation process of the grout, as well as the temporal variation of the grout viscosity, should be considered altogether.

In this work, a novel model to characterise the temporal and spatial distribution of the grout pressure in the tail void is proposed, based on the theory of group diffusion and consolidation. The temporal variation of the grout viscosity is also considered in the proposed model. The proposed model is first verified against monitored real grout pressure measured at different locations in a big-diameter cross-river road tunnel project in China. Then a three-dimensional finite element model of the lining segments is developed to study the effects of the grout pressure on the mechanical response of the lining segments. The mechanical responses of the lining segments, in terms of internal force, moment and stress profile, are thoroughly analysed. These mechanical responses are also verified against the field monitored data, to further validate the proposed model of grout pressure distribution. The study in this work provided important guidance to the grouting process and refined quality control of the tunnel lining segments during the field construction.

2. Three-dimensional spatial distribution of the grout pressure

The grouting process consists of two major phases, (1) diffusion phase, in which the grout is being injected into and diffusing and filling up the rock-segment void simultaneously when the lining segments is being pushed out of the shield tail; (2) consolidation phase, in which the grout is being consolidated under the confining effect from the surrounding rock, meanwhile the grout pressure is dissipating. In this section, the three-dimensional spatial distribution of the grout pressure at the end of first phase is formulated.

2.1. The grout pressure distribution along circumferential direction

After being injected into the segments-rock void, the grout diffuses from the grouting holes to the remaining void, and an annular grout cake will be generated ('annular cake' for short), as shown in Figure 1. The radial thickness (T) of annular cake is much larger than the longitudinal width (W), which is equal to the shield advance distance during the time period of grout diffusion.

The circumferential distribution of the grout pressure p_r is a function about the angle α, which can be calculated as (Gou, Ye, & Zhang, 2013)

$$p_r = p_{G0} + X(\cos\alpha_i - \cos\alpha) \pm Y(\alpha_1 - \alpha) \tag{1}$$

where p_{G0} is initial grouting pressure at the ith grouting hole, α_i is the angle between ith grouting hole and y axis, α_1 indicates position of grouting hole 1 showing in Figure 1, X and Y are the parameters about grout weight and shear stress, respectively, and it takes '+' if the grout filling downward along the shield tail void, '−' if filling upward.

$$X = \rho g R \tag{2}$$

where ρ is grout density, g is the gravity acceleration and R is external radius of tunnel lining segments. Assuming that the flowing grout is Bingham fluid, then parameter Y can be gotten as follows:

$$Y^3 - \left(\frac{3R\tau_0}{W} + \frac{12R\mu_0 q}{TW^3}\right)Y^2 - \frac{4R^3\tau_0^3}{W^3} = 0 \tag{3}$$

where τ_0 is the stationary shear stress of grout, μ_0 is the Bingham plastic viscosity of unconsolidated non-aged grout, q is grout flux injected into the tail void within the given time period.

2.2. The grout pressure distribution along longitudinal direction

The diffusion of grout along longitudinal direction in the rock-segment void lasts for hours (Fan, Han, & Fang, 2011). Figure 2 shows the schematic diagram of grout diffusing along the longitudinal direction. In order to formulate the grout pressure distribution along the longitudinal direction, the following assumptions are made:

- The grout fills up 'annular cake' rapidly when diffusing along the circumferential direction (Figure 1). Then the 'annular cake' diffuses, as a whole, along the longitudinal direction.
- During longitudinal diffusion process, the grout remains Bingham fluid.
- The grout flow will not be affected or blocked by the grout filled previously.

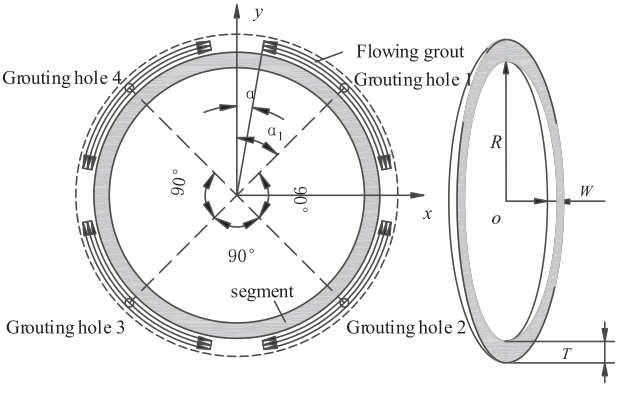

Figure 1. Schematic diagram of the grout diffusing along circumferential direction.

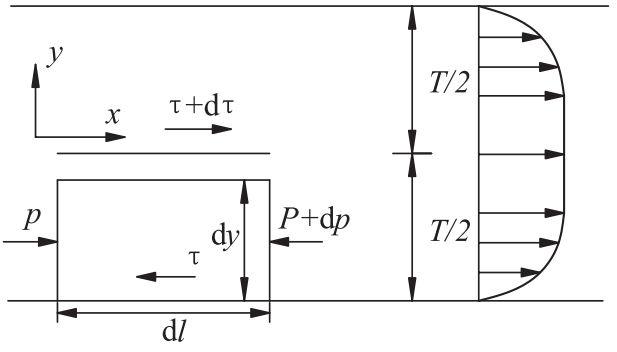

Figure 2. Schematic diagram of grout diffusing along the longitudinal direction.

Let p_l be the longitudinal grout pressure, dl be the finite length along x direction, dy be the finite length along transverse direction, τ be the grout shear stress and T be the filling thickness of grout. The force equilibrium along x direction of the finite volume gives,

$$p_l \mathrm{d}y - (p_l + \mathrm{d}p_l)\mathrm{d}y - \tau \mathrm{d}l + (\tau + \mathrm{d}\tau)\mathrm{d}l = 0 \tag{4}$$

After rearrangement, one can arrive at the following relation,

$$\frac{\mathrm{d}\tau}{\mathrm{d}y} = \frac{\mathrm{d}p_l}{\mathrm{d}l} \tag{5}$$

Let $\mathrm{d}p_l/\mathrm{d}l = Z$, and recall boundary conditions that at the location of grouting holes: $l = 0$, $p_l = p_{G0}$ (the initial grout pressure), the grout pressure distribution along longitudinal direction can be given as,

$$p_l = p_{G0} + Zl \tag{6}$$

Similar as Equation (3), the parameter Z can be calculated by

$$Z^3 - \left(\frac{3\tau_0}{T} + \frac{12\mu q}{T^3}\right)Z^2 + \frac{4}{T^3}\tau_0^3 = 0 \tag{7}$$

3. Mechanism of grout consolidation and pressure dissipation

The consolidation process of the grout involves two major periods, at first certain amount of cement seeps out of the grout aggregates, and then secondly the cement permeates into the surrounding rock. In this section, the grout consolidation and pressure dissipation mechanisms in each period are analysed, respectively.

3.1. Grout consolidation under the confining effect from surrounding rock

3.1.1. The osmotic pressure of the grout layer

To begin with, the osmotic pressure of the grout layer during the grout consolidation process is derived. During the grouting process, the surrounding rock will experience two phases of deformation. The first phase of deformation takes place immediately after the lining segments is pulled out of the shield tail. In this phase, the grout is synchronously injected into and fill up the rock-segment void. At the end of this phase, mechanical equilibrium is established at the grout and rock mass interface,

$$p_g = \sigma' + p_p \tag{8}$$

where p_g is grouting pressure, σ' is the radial effective stress of rock mass and p_p is the pore water pressure inside the rock mass. The second phase of deformation is a fairly long process along with the

consolidation of the grout layer. In this phase, the rock mass exhibits the same amount of deformation as the reduced thickness of the grout layer due to grout consolidation. Figure 3 shows a schematic diagram of the grout layer, surrounding rock and corresponding deformation.

Assuming the rock mass is homogeneous, isotropic and self-supported after disturbed, the deformation of the rock mass is in elastic region, and the interface contact effect between the grout layer and segments is negligible. Denote the thickness of the disturbed rock mass as r, and the thickness of the grout layer as δ. The particular component of the deformation being of interest is the radial deformation, i.e. the deformation that the rock mass moves towards the grout, Δr shown in Figure 3. According to the generalised Hooke's law, the radial strain increment of the disturbed rock mass under plane strain condition can be given as,

$$\Delta\varepsilon_r = \frac{1-\nu^2}{E}\left(\Delta\sigma_r - \frac{\nu}{1-\nu}\cdot\Delta\sigma_\theta\right) \tag{9}$$

where $\Delta\sigma_r$ and $\Delta\sigma_\theta$ are the radial stress increment and circumferential stress increment of disturbed rock mass, respectively, E is elasticity modulus, and ν is Poisson ratio. As $\Delta\sigma_\theta \approx 0$, Equation (9) can be rewritten as,

$$\Delta\sigma_r = \frac{2G}{1-\nu}\frac{\Delta r}{r} \tag{10}$$

where

$$\Delta\varepsilon_r = \frac{\Delta r}{r} \tag{11}$$

$$G = \frac{E}{2(1+\nu)} \tag{12}$$

and Δr is radial deformation of disturbed rock mass, G is shear modulus of disturbed rock mass.

To this end, the osmotic pressure p of the grout layer, i.e. the pressure difference between the grout in the grout layer and pore water in the rock mass, which is also equivalent to the effective stress of the rock mass, can be obtained,

$$p = \sigma' = \sigma'_0 - \Delta\sigma_r = p_0 - \frac{2G}{1-\nu}\frac{\Delta r}{r} \tag{13}$$

where p_0 denotes the initial osmotic pressure, which is equivalent to the initial radial effective stress σ'_0 of the rock mass.

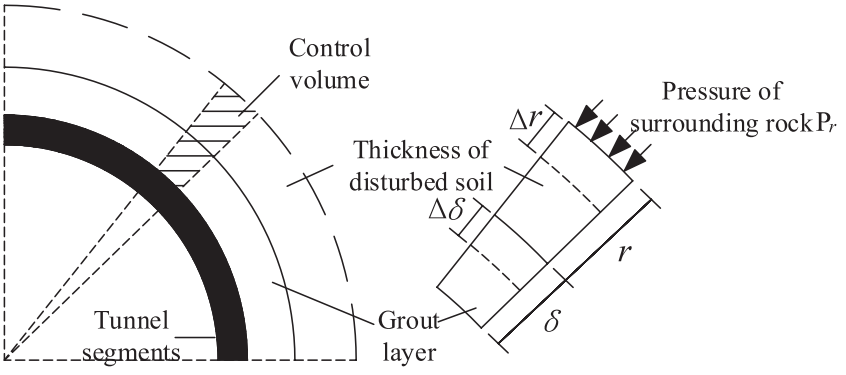

Figure 3. Schematic diagram of the grout layer, surrounding rock and corresponding deformation.

3.1.2. Formulation of grout consolidation

It is assumed that the grout layer is consolidated, i.e. dehydrates and hardens gradually from the grout–rock interface. Denote the thickness of the consolidated grout layer as x, and the grout permeability of the consolidated grout layer as k. The grout flux q_c that flows through the consolidated grout layer can be given based on Darcy's law,

$$q_c = k\frac{\Delta h}{x} \tag{14}$$

where Δh is the pressure head difference, i.e. the osmotic pressure, recalling of Equation (13), which can be given as

$$\Delta h = \frac{\Delta p}{\rho g} = \frac{1}{\rho g}\left[p_0 - \frac{2G}{1-\nu}\frac{\Delta r}{r}\right] \tag{15}$$

The grout flux can be also derived from the volume change in the consolidated grout layer, as

$$q_c = \left(\frac{n_i}{1-n_i} - \frac{n_e}{1-n_i}\right)\frac{\mathrm{d}x}{\mathrm{d}t} = \frac{n_i - n_e}{1-n_i}\frac{\mathrm{d}x}{\mathrm{d}t} \tag{16}$$

where n_i is the initial porosity of the grout, and n_e is the porosity of the consolidated grout layer. Combing Equations (14)–(16) gives,

$$\frac{x}{k}\frac{\mathrm{d}x}{\mathrm{d}t} = \frac{1-n_i}{n_i - n_e}\frac{1}{\rho g}\left[p_0 - \frac{2G}{1-\nu}\frac{\Delta r}{r}\right] \tag{17}$$

In order to solve Equation (17), one more relation is required to be established between the variables x and Δr. With recourse to the geometrical compatibility of the grout layer and rock deformation, the following relation can be arrived, that the ratio of Δr to x should be equal to the ratio $n_i - n_e$(porosity variation before and after consolidation) to $1 - n_i$ (volume rate of solid in grout),

$$\frac{\Delta r}{x} = \frac{n_i - n_e}{1-n_i} \tag{18}$$

Combing Equations (17) and (18), and solve for x gives,

$$\frac{x}{k}\frac{\mathrm{d}x}{\mathrm{d}t} + \frac{2}{\rho g}\frac{G}{r}\frac{1}{1-\nu}x = h_0\frac{1-n_i}{n_i - n_e} \tag{19}$$

where $h_0 = \frac{p_0}{\rho g}$, is initial pressure head difference corresponding to initial osmotic pressure.

Let $B = \frac{2G}{\rho g r}\frac{1}{1-\upsilon}$, $C = \frac{1-n_i}{n_i - n_e}$, then Equation (19) can be rewritten as,

$$\frac{x}{k}\cdot\frac{\mathrm{d}x}{\mathrm{d}t} + Bx = Ch_0 \tag{19b}$$

Substitute Equation (18) into Equation (13), the osmotic pressure can be solved as

$$p = p_0 = -\frac{2G}{1-\nu}\frac{1}{r}\frac{n_i - n_e}{1-n_i}x(t) \tag{20}$$

3.2. Effect of flow resistance from the surrounding rock mass on the grout pressure dissipation

The derivation in the previous subsection implicitly assumed that, the grout seepages out from the grout layer will flow freely into the surrounding rock mass. It is not necessary true since there is flow resistance from the rock mass. Herein, the flow resistance f is defined as ratio of flow distance to the grout permeability, or the ratio of pressure head drop to the flux,

$$f = \frac{\Delta h_f}{q_f} = \frac{L_f}{k_f} \tag{21}$$

where Δh_f is the pressure head difference, q_f is the flow flux, L_f is the flow distance and k_f is the grout permeability, generally.

Taking the grout flow through consolidated grout layer as an example, the flow resistance from the consolidated grout layer can be given as,

$$f_g = \frac{x}{k} \tag{22}$$

Similarly, the flow resistance from the rock mass when grout is permeating through the rock mass can be given as,

$$f_s = \frac{\Delta h_s}{q_s} \tag{23}$$

In the cross section, the grout discharge Q_g that flows out of the grout layer can be calculated from

$$Q_g = 2\pi R q_g \tag{24}$$

where R is the tunnel radius, and q_g is the flow flux out of the grout layer. The grout discharge Q_s that flows through any cross sections in the rock mass can be calculated from

$$Q_s = 2\pi r q_s = 2\pi r k_s \frac{\mathrm{d}h_s}{\mathrm{d}r} \tag{25}$$

where r is the polar radius at the cross section being considered (seen Figure 4), k_s grout permeability of the rock mass, and $\frac{\mathrm{d}h_s}{\mathrm{d}r}$ represents the pressure head gradient at that cross section.

Notice that the grout discharge Q_g that flows out of the grout layer is exactly equal to the grout discharge Q_S that flows through the cross sections in the rock mass. Let $Q_g = Q_S$, and one can get

$$\frac{\mathrm{d}r}{r} = \frac{k_s}{R q_g}\mathrm{d}h \tag{26}$$

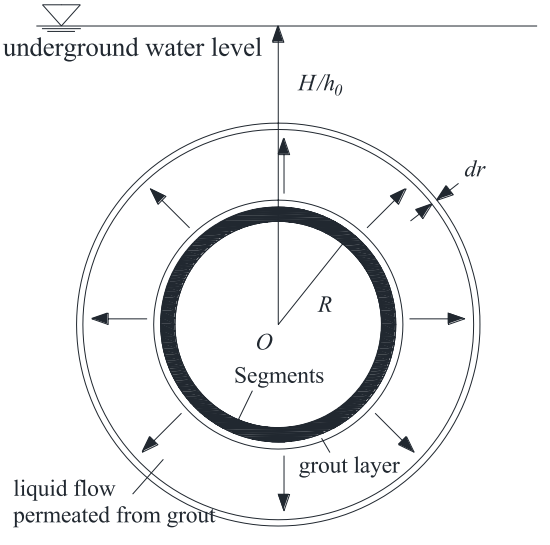

Figure 4. Grout flowing through the surrounding rock mass.

Recall the boundary conditions that, $r = R$, $h = 0$; $r = H$, $h = h_s$. Solve Equation (26) for h and substitute into Equation (23), one can obtain the flow resistance of the rock mass

$$f_s = \frac{\Delta h_s}{q_s} = \frac{R}{k_s} \ln \frac{H}{R} = \frac{F}{k_s} \tag{27}$$

where $F = R \cdot \ln (H/R)$.

Analogous to Equation (19b), the thickness of the consolidated grout layer, considering the flow resistance from the rock mass, is modified to

$$(f_g + f_s)\frac{\mathrm{d}x}{\mathrm{d}t} + Bx = Ch_0 \tag{28}$$

3.3. Effect of temporal variation of grout viscosity on the rock mass grout permeability

As the grout in the rock mass gradually dehydrates and hardens, the viscosity of the grout is increasing, which further results in the reduce of grout permeability of the rock mass, seen Figure 5.

In this work, an exponential evolution of the grout viscosity $\mu(t)$ is adopted

$$\mu(t) = \mu_0 e^{\xi t} \tag{29}$$

where μ_0 is the grout initial viscosity, and ξ is a material constant, which can be obtained from experiment.

The grout permeability of the rock mass, considering the variation of grout viscosity, is given by

$$k_s(t) = k_w / \beta(t) \tag{30}$$

where k_w is water permeability in surrounding rock, $\beta(t)(\beta(t) = \mu(t)/\mu_w)$ is the ratio of grout viscosity to water viscosity. Substituting Equation (29) into Equation (30) gives

$$k_s(t) = k_w \cdot \frac{\mu_w}{\mu_0} \cdot e^{-\xi t} = \frac{k_w}{\beta_0} \cdot e^{-\xi t} \tag{31}$$

Then Equation (28) can be rewritten as

$$\left(\frac{x}{k} + \frac{F}{k_s(t)}\right)\frac{\mathrm{d}x}{\mathrm{d}t} + Bx = Ch_0 \tag{32}$$

Then the consolidated grout thickness $x(t)$ can be obtained by solving Equation (32), given the initial condition that $t = 0$, $x = 0$.

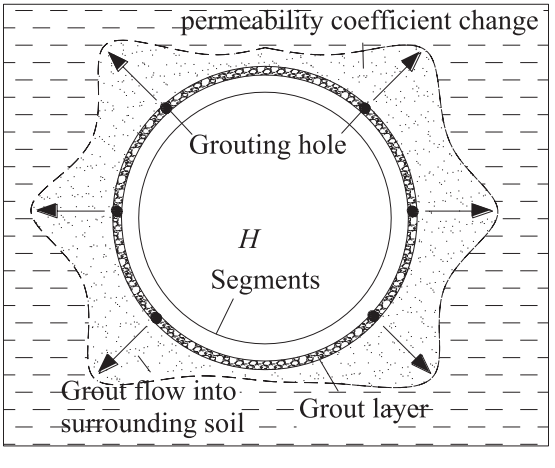

Figure 5. Rock mass permeability changed by grout diffusion.

Finally, recalling Equations (8) and (20), the grouting pressure can be given by

$$p_{gt} = p_{r,l} = \frac{2G}{1-\nu}\frac{1}{r}\frac{n_i - n_e}{1 - n_i}x(t) \tag{33}$$

where p_{gt} is the grouting pressure at time, $p_{r,l}$ is the grouting pressure at the end of diffusion process, which can be calculated from Equations (1) and (6).

4. Verification of the proposed temporal and spatial grout pressure distribution

The proposed temporal and spatial grout pressure distribution model is applied to a field tunnel project to characterise the grout pressure distribution within the grout layer.

4.1. Project description and grouting parameters

The tunnel studied in this work is Nanhu road shield tunnel, a big-diameter cross-river road tunnel, located beneath the Xiangjiang river in Changsha, Hunan, China, as shown in Figure 6. The particular cross section of the tunnel concerned in this work lies under the river, where the surrounding rock mainly consists of moderately weathered conglomerate, and the overlying rock is strong weathered conglomerate.

The grout is injected from the shield tail into the rock-segment gap, through four grouting holes, 45°, 135°, 225° and 315° to the *y* axis, as shown in Figure 7. The grout parameters and grouting settings are listed in Tables 1 and 2.

4.2. Determine the temporal variation of the grout viscosity

Grout viscosity rheological test is conducted to obtain the temporal variation of the grout viscosity. The test procedure (shown in Figure 8) is simply described as following,

(1) Collect and mix all ingredients of the grout with corresponding weight ratio given in Table 3.
(2) Collect five cups of mixed grout, label with index and time, respectively.
(3) Pour each cup of grout sample into viscometer, adjust the shear rate scheme of viscometer.
(4) Start rotating, take down the shear stress of the grout every 10 min (60 min in total).
(5) Calculate the grout viscosity based on the recorded shear stress and shear rate.

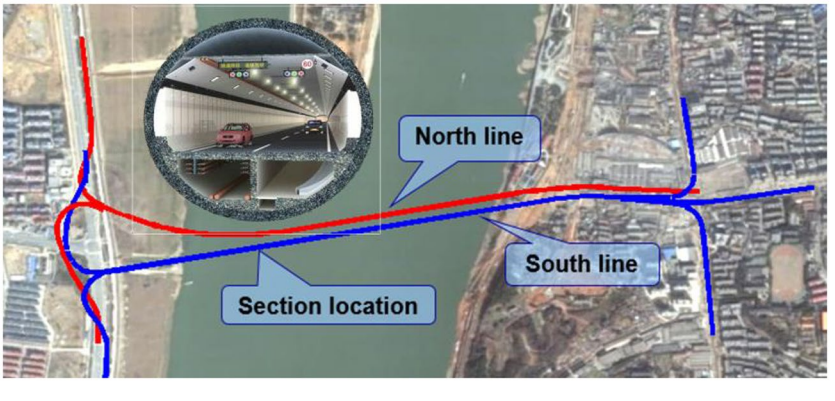

Figure 6. Nanhu road shield tunnel in Changsha, Hunan, China.

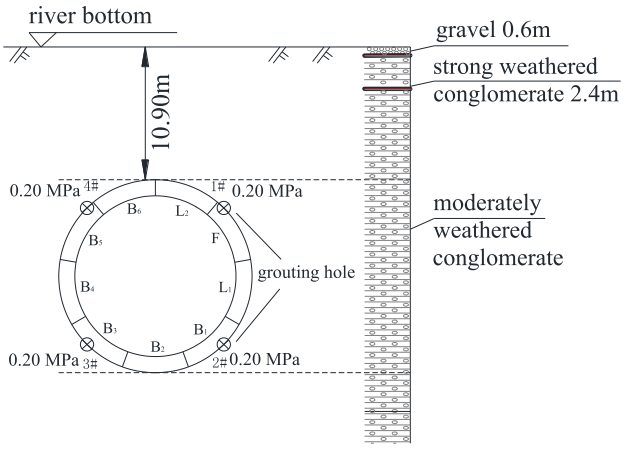

Figure 7. The cross section of the shield tunnel and typical geological layer.

Table 1. Main physical and mechanical properties of the grout used in the shield tunnel project.

Bleeding rate[a]	Hardening time[b]/h	Fluidity[c]/cm	Cohesion/kPa	Friction angle (24 h)/°	Compressive strength/MPa	Compression modulus/MPa
6.6%	7	23.5	0.5 (24 h)	31.4 (24 h)	4.56 (28 d)	24.4 (40 h)

[a]The volume ratio of the permeated water and consolidated grout, measured by measuring cylinder.
[b]The time when the fresh grout turns into consolidated one, measured by vicat apparatus.
[c]Pour the fresh grout on the 'jump table', the table will vibrate 30 times in 30 s. After that, measure the diffusion diameter of grout and calculate the AVG of that, which is called the grout fluidity.

Table 2. Grout parameters and grouting settings used in Nanhu road shield tunnel.

Advance rate s/(m/s)	segment radius R/m	Tail void thickness T/m	Initial grouting pressure p_0/MPa	Grout flow q/m^3/s	Initial pressure head h_0/m
0.00035	5.65	0.165	0.2	3.9×10^{-4}	6.68
Grout density ρ/(kg/m^3)	Plastic viscosity μ/Pa s	Static shear force τ_0/Pa	Initial grout porosity n_i	Grout cake porosity n_e	Initial grout permeability coefficient k_0/(m s^{-1})
1900	2	270	0.425	0.417	4.7×10^{-8}

The grout viscosity at different time is plotted in Figure 9. The exponential evolution of the grout viscosity with time given in Equation (29) is used to fit the experiment data. The fitting result is $\mu(t) = 0.907e^{0.0107t}$.

4.3. Grout pressure distribution evaluated from proposed model

The grout pressure distribution is evaluated from Equation (33), given the parameters in the previous subsections. The results of two cases are presented: (1) without varying viscosity and (2) with varying viscosity.

The results of grout pressure distribution at the TBM along the circumferential direction are presented in Figure 10. For both cases, the grout pressure is nonlinear distributed along the segment circumference, with the top and middle areas presents fairly low pressure. Such distribution pattern makes sense, since the gravity significantly drives the grout downward. The grout pressure is dissipating with time, and the dissipating rate is decreasing with time. If the temporal varying viscosity is considered, the grout permeability of the rock mass would decrease with the increasing grout

Figure 8. Grout viscosity rheological test.

Table 3. Grout mix design: ingredients and corresponding weight (unit: kg).

Cement	Coal ash	Bentonite	Sands	Water	Additives
187.0	313.0	49.6	770	375.0	5.0

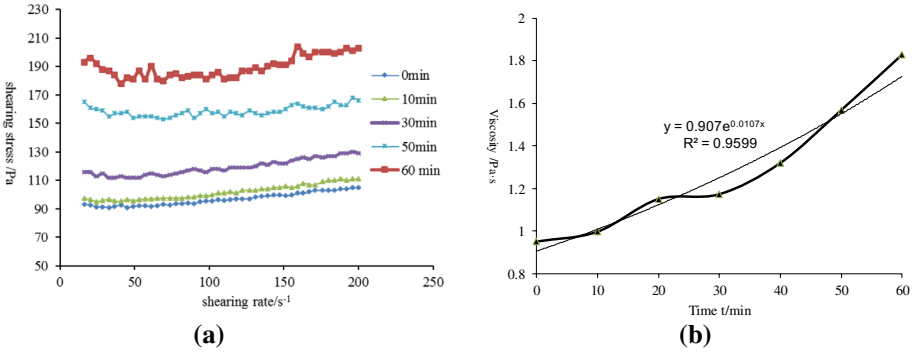

Figure 9. Temporal variation of the grout viscosity evaluated from laboratory: (a) the recorded shear stress vs. shear rate at different time and (b) the fitting results of the temporal variation of the grout viscosity.

viscosity, thus slowing down the pressure dissipation of the grout. This can be observed from the fact that, the grout pressure decreases by 19.4% at $t = 7500$ s if varying viscosity is considered, compared to 35.6% if not.

In order to verify the accuracy of the proposed model in characterising the grout pressure distribution in the grout layer, the results are benchmarked against filed monitored data of the grout pressure. Figure 10 shows the pressure variation as a function of time monitored at different locations. It can be seen that all the pressure decreases about 9.5% ~ 25.5% and goes stable later on. The amount of pressure decrease matches better with the pressure distribution model with varying viscosity (Figure 11).

Similarly, the grout pressure distribution along longitudinal direction is also evaluated, and the results are presented in Figure 12. In both cases, the pressure decreases linearly with distance away from the grouting cross section. The grout pressure at different locations along the longitudinal direction all decreases by the same rate with time going on, i.e. the pressure–distance line moves downward parallel. It can be observed that, if not considering varying viscosity, the grout pressure decreases by

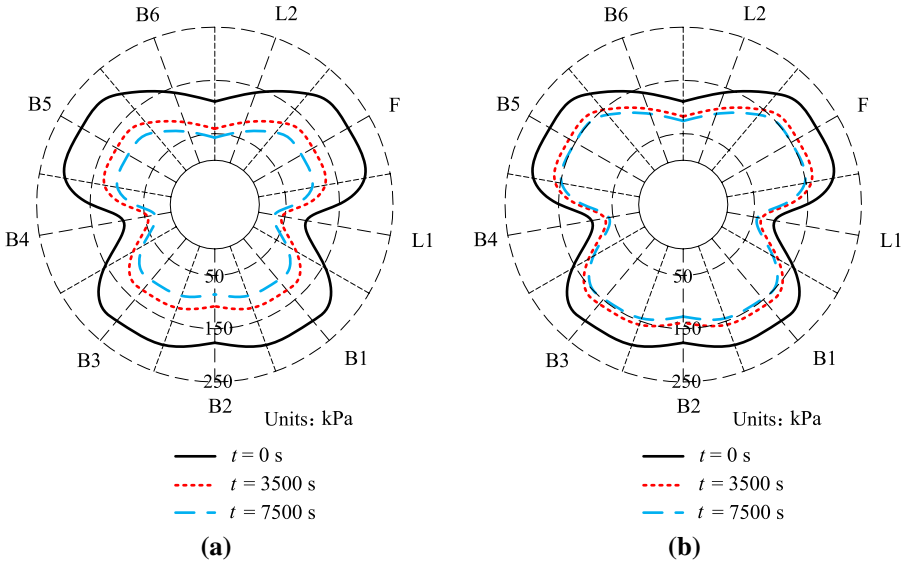

Figure 10. Grout pressure distribution at the TBM along circumferential direction at different time (a) without varying viscosity and (b) with varying viscosity.

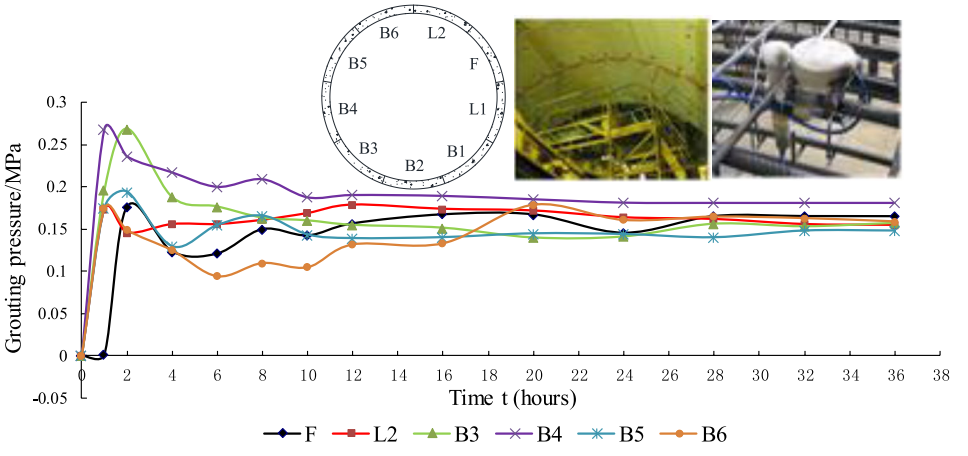

Figure 11. Grout pressure at different locations monitored in field.

25.6% and propagates about 8 m at the end of grouting process; if considering varying viscosity, the grout pressure decreases by 13.3% and propagates about 9.4 m.

5. Effects of grout pressure on the mechanical response of lining segments

The grout pressure distribution is of great influence to the mechanical response, in terms of the internal force, moment and stress of the lining segments. In this section, a three-dimensional finite element model is developed to simulate the mechanical response of the lining segments applied with temporal and spatial distributed grout pressure. The simulated mechanical response of the lining segments is benchmarked against field monitored data, to further validate the proposed model of grout pressure distribution.

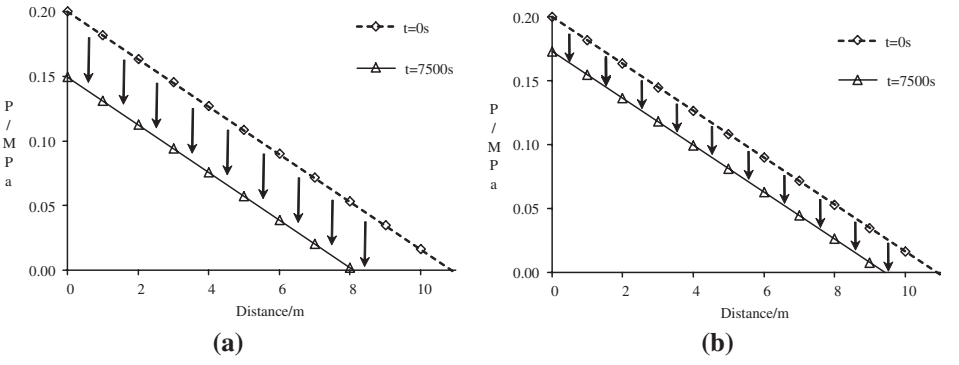

Figure 12. Grout pressure distribution along longitudinal direction versus the diffusion distance, in the case of $t = 0$ and $t = 7500$ s: (a) w/o varying viscosity and (b) w/ varying viscosity.

Table 4. Model geometry and material properties.

Outer diameter	Division of segments ring	Segment width	Segment thickness	Segment elasticity modulus	Segment Poisson ratio
11.3 m	9	2.0 m	0.5 m	35,000 MPa	0.2
Linking bolts elasticity modulus	Linking bolts Poisson ratio	Combin14 spring constant	Combin39 spring constant	Conglomerate elasticity modulus	Conglomerate Poisson ratio
210,000 MPa	0.31	50,000 kN/m	16,400–67,200 kN/m	11,000 MPa	0.22

5.1. Model domain, boundary conditions and material properties

The software ANSYS is adopted to study the three-dimensional mechanical response of the lining segments. The 3D FEM model contains six rings of segments in the longitudinal direction, and each ring consists of nine single segments. The outer diameter of the ring segments is 11.3 m, the thickness is 0.5 m and the longitudinal length is 2.0 m. The model geometry is also listed in Table 4.

The segments are modelled with shell element (shell63). The contact behaviours, i.e. bending, shearing and compressing, between the segments are modelled with spring elements: contacts between segments within the same ring are modelled with combin39, and the contacts between segments within different rings are modelled with combin14. The linking bolts between the segments within different rings are modelled with tension only bar element (link10). The contact behaviour between the segments and surrounding rock is modelled with compression only bar element (link10). All the materials are considered as linear elastic, and the material properties of the segments, contacts and linking bolts are listed in Table 4.

The load from earth and pore water pressure is applied on the circumferential surface of the segments as pressure boundary condition, as shown in Figure 13, and the pressure magnitudes is listed in Table 5. The compression force from the cylinder thrust of the shield is about 165 MPa in longitudinal direction, and is applied to the lateral surface of the first ring. The time-dependent grout pressure, as evaluated in Section 4.2, is applied on the circumferential surface of the segments.

Since the dissipation of the grout pressure is a fairly long process, the dynamic simulation of the developed FEM model would be great computational expensive. For our contribution, the static solid mechanics solver is adopted, with varying the applied grout pressure in each simulation. It makes sense since that, the grout pressure variation is fairly slow so that the grout pressure can be considered as static load at a given time. The simulation procedure is briefly described as following,

(1) Delete the grout pressure previously applied on the segments, if any.
(2) Evaluate the grout pressure at given time t ($t = 0$s, Δt, $2\Delta t$, $3\Delta t$, …, 7500 s), where Δt is the time interval.

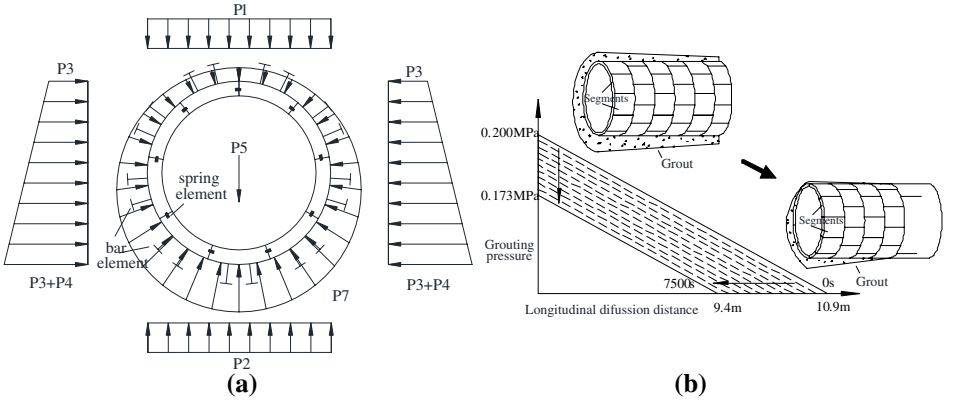

Figure 13. The load scheme of (a) earth and pore water pressure, and (b) grout pressure.

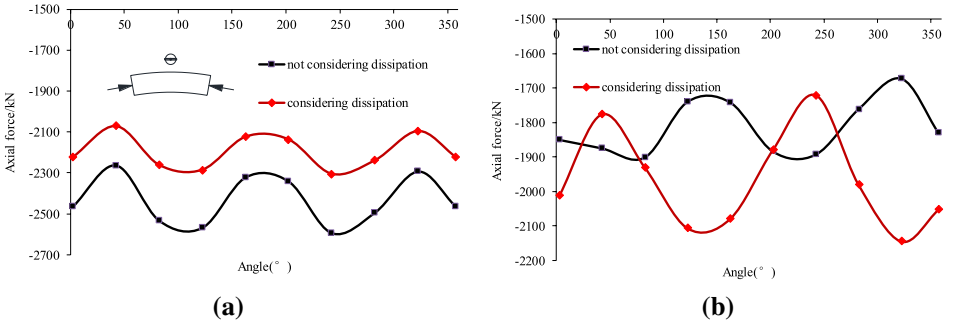

Figure 14. Axial force profile within the segment rings at $t = 7500$ s: (a) the first ring and (b) the fifth ring.

Table 5. The load magnitudes of the earth and pore water pressure shown in Figure 13(a).

Load indices	P1	P2	P3	P4	P5	P7*
Load value	103.6	498.3	29.0	29.4	5.0	/

Note*: P7 is the water buoyancy, the calculation formula is: $P_7 = \gamma_w (H_w + R - R\cos\varphi)$, where γ_w is the water unit weight and H_w is the height of water head at the top of tunnel.

(3) Applied the grout pressure at time t on the segments and solve the model.
(4) Repeat step (1), (2) and (3) for every time step.

The aforementioned procedure is implemented with APDL to simulate all the time steps in batch.

5.2. *Effect of grout pressure on the mechanical response of the segments*

To begin with, the internal forces, i.e. axial force and bending moment, of the segments are studied. The two cases of models, case I that without grout pressure dissipation and case II that with grout pressure dissipation, are considered. Figure 14 shows the axial force profile along the circumferential direction in the segments within the first ring and fifth ring. In the first ring, the axial force profiles of both cases are almost parallel to each other. The axial force of case II is about 9% lower than that of case I, due to the lower grout pressure after dissipation. The variation pattern of axial force profiles of the two cases in the fifth ring is totally different from each other. It can be observed that, for case I, the axial force profile in the fifth ring is almost coincident with the axial force profile in the first ring.

However, the axial force profile in the fifth ring of case II is much different. It is worth noting that, if considering grout pressure dissipation, i.e. in case II, the grout pressure cannot propagate to the fifth ring, recalling Figure 12(a). It is the absence of the grout pressure that makes the big difference to the axial force profile in the fifth ring. The axial force profile of case II exhibits greater fluctuation along the circumferential direction, and overall larger force magnitude, which may also due to the absence of grout pressure in the fifth ring.

The bending moments profile along the circumferential direction in the segments are shown in Figure 15. In the both rings, the bend moment profiles of both cases are almost coincident with each other. In the first ring, the bending moments of case II are overall 30% smaller than that of case I, due to the lower grout pressure after dissipation. In the fifth ring, the bending moments of case II are little bit larger than that of case I, which is consistent with the phenomenon discussed in Figure 14(b).

To better understand how the grout pressure affects the stability of the segments, the stress profile in the segments is studied. The principal stress contours of the two cases are plotted in Figure 16. For case I, in which the pressure dissipation is not considered, both the major and minor principle stresses in the first four rings are larger and more heterogeneously distributed than that in the last two rings. Most area in the first four rings is subjected to compressive stress in the principal stress direction, with only small area at top and bottom vicinity subjected to tensile stress ranging from 0.22 to 5.71 MPa. For case II, the minor principal stress in all rings is larger than that of case I.

5.3. Benchmark against field monitored data

In field, the earth pressure cell, pore water pressure cell and concrete strain metre are placed at assigned locations in the lining segments. The bending moment and stress in the segments are monitored during the grouting process. Some monitoring results compared with numerical results are presented in Table 6.

It can be seen that the bending moment in field is smaller than that evaluated from numerical model. It may due to the fact that, when the segments are pushed out of the shield tail, the surrounding rock (moderately weathered conglomerate) would not fill up the rock-segment void immediately benefit from the self-stability of the rock, which results in smaller load applying on the lining segments. Contractionary, all the load of the surrounding rock is supposed to be applying on the lining segments in the numerical model, which leads to segments subjecting to larger bending moment. Nevertheless, case II in which the grout pressure dissipation is considered matches better with the field monitored data than case I. Case II also gives better characterisation of the maximum tensile stress.

According to the numerical results, the tension damage always occurred at ±45° and ±135° of segments close to the shield tail, especially at the corner of segments, circumferential or longitudinal seam and joints, which is consistent with the actual damage locations in field construction (as shown in Figure 17). Particular attention should be paid to such locations in the segments during field construction.

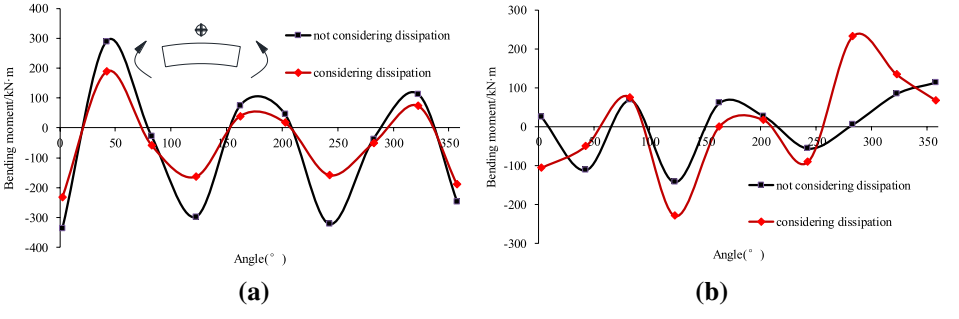

Figure 15. Bending moment profile within the segment rings at t = 7500 s: (a) the first ring and (b) the fifth ring.

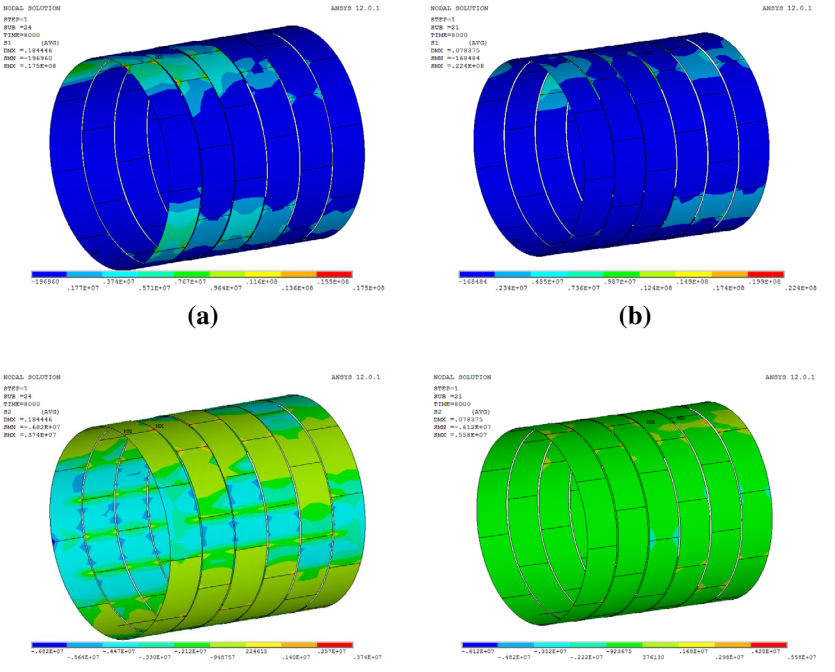

Figure 16. Major and minor principal stress distribution of the two cases. (a) Major principal stress w/o considering dissipation. (b) Major principal stress w/ considering dissipation. (c) Minor principal stress w/o considering dissipation. (d) Minor principal stress w/ considering dissipation.

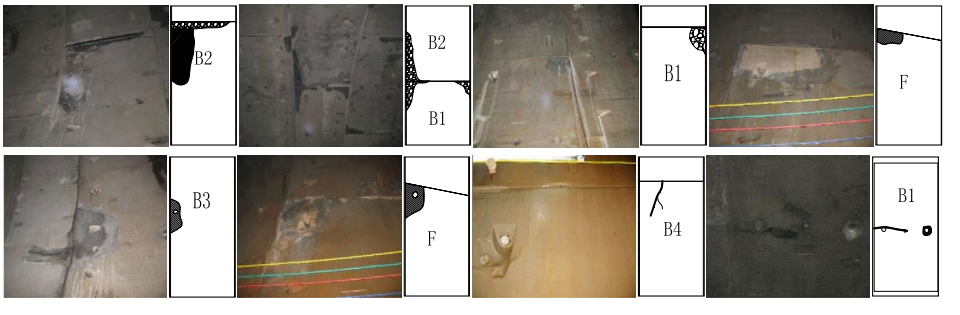

Figure 17. Segment damage conditions in field construction.

Table 6. Comparison of numerical and field monitoring results.

	Maximum positive moment/kN m	Maximum negative moment / kN m	Maximum tensile stress/MPa
Field results	168.7	−140.0	1.35
Case I	290.8	−335.7	0.22–5.71
Case II	189.4	−230.7	0.37–2.34

6. Conclusion

The grouting process is of great importance to the stability of lining segments in shield tunnelling. This work proposed a novel model to characterise the temporal and spatial distribution of the grout pressure in the rock-segment void, based on the theory of group diffusion and consolidation. The effect

of varying grout viscosity is also, for the first time, taken into consideration in studying the evolution of grout pressure. A 3D FEM model of the lining segments is developed, and applied with the proposed model of the grout pressure distribution. The mechanical response of the lining segments, in terms of internal force, bending moments and stresses, are thoroughly analysed. And the results evaluated from the numerical model are benchmarked against field monitored data. Summarising the results in this work, the following conclusions are made,

(1) The temporal and spatial distribution of grout pressure can be well characterised by the proposed model, which is derived based on the diffusion and consolidation theory, as well as considering the temporal variation of grout viscosity.
(2) Along the circumferential direction, the segments are subject to greater grout pressure at vicinity of grouting holes, and smaller grout pressure at the 'waist' area. The grout pressure at the lower part of the segments is greater than that at upper part. The grout pressure is linearly decreasing along the longitudinal direction. The increase in the grout viscosity slows down the grout diffusion, consolidation and pressure dissipation. The grout pressure vanishes at a further distance as a result of increasing viscosity.
(3) The developed 3D FEM model presents well prediction of the mechanical response of the lining segments. The internal force, bending moments and stress in the segments are overall smaller, and less fluctuating if the grout pressure dissipation is considered in the FEM model. The mechanical response of the fifth ring is greatly impacted by the condition of grout pressure.
(4) Special attention should be paid to the area of grouting holes, segment corners, seam and joints in the field construction, based on the simulation results of the developed 3D FEM model.

This work provides significant information to the field construction of the shield tunnel. However, it should be pointed out that, compression effect of surrounding rock on grout is not considered. Thus, the proposed formulation of the grout pressure distribution suits well for the surrounding rock in good quality with well self-stability. Its application for sandy, sof, and clay-like rock should be further studied.

Disclosure statement

No potential conflict of interest was reported by the authors.

Funding

This work was supported by the National Natural Science Foundation of China [grant number 51678578], [grant number 51108472]; the Guangdong Natural Science Foundation of China [grant number 2016A030313233]; the Guangdong Provincial Science & Technology Program of China [grant number 2015A020217004]; the Guangzhou Science & Technology Program of China [grant number 201704020139]; and the Department of Communications of Guangdong Province of China [grant number 2016-02-026].

ORCID

Z. S. Lai http://orcid.org/0000-0002-2378-9193

References

Bai, Y., Dai, Z. R., & Zhang, S. S. (2011). Study on the grout pressure dissipation mode in simultaneous backfill grouting during shield tunneling. *China Railway Science, 32*, 38–45.

Bezuijen, A., & Talmon, A. M. (2006). Grout pressures around a tunnel lining, influence of grout consolidation and loading on lining. *Tunnelling and Underground Space Technology, 9*, 443–444.

Bezuijen, A., Talmon, A. M., Kaalberg, F. J., & Plugge, R. (2004). Field measurements of grout pressures during tunnelling of the sophia rail tunnel. *Soils and Foundations, 44*, 39–48.

Do, N., Dias, D., & Oreste, P. (2014). Three-dimensional numerical simulation for mechanized tunnelling in soft ground: The influence of the joint pattern. *Acta Geotechnica, 9*, 673–694.

Fan, Z. P., Han, Y. W., & Fang, Z. Q. (2011). Calculating model of backfill grouting pressure distribution for shield tunnel. *Journal of Highway and Transportation Research and Development, 28*, 95–100.

Gou, C. F., Ye, F., & Zhang, J. L. (2013). Ring distribution model of filling pressure for shield tunnels under synchronous grouting. *Chinese Journal of Geotechnical Engineering, 35*, 591–598.

Han, Y. W., Zhong, X. C., & Yu, X. F. (2007). Experimental research on the backfill grout deformation and grout pressure dissipation of Shield Tunnel. *Chinese Journal of Underground Space and Engineering, 3*, 1142–1147.

Hashimoto, T., Nagaya, J., Konda, T., & Tamura, T. (2002). Observation of lining pressure due to shield tunnelling. In *Proceedings of the 3rd International Symposium on Geotechnical Aspects of Underground Construction in Soft Ground, ISSMGE-TC28* (pp. 119–124). Toulouse.

Huang, L. C., Xu, Z. S., & Zhou, C. Y. (2009). Modeling and monitoring in a soft argillaceous shale tunnel. *Acta Geotechnica, 4*, 273–282.

Kasper, T., & Meschke, G. (2006). On the influence of face pressure, grouting pressure and TBM design in soft ground tunnelling. *Tunnelling and Underground Space Technology, 21*, 160–171.

Liang, Y., Su, W. H., & Fang, L. G. (2014). Field test and analysis on stress of lining of large-diameter river river-crossing shield tunnel. *Tunnel Construction, 34*, 637–641.

Lin, J. X., Yang, F. Q., Shang, T. P., & Xie, B. (2008). Study on tunnel stability against uplift of super-large diameter shield tunneling. In R. Huang (Ed.-in-Chief), *The Shanghai Yangtze River Tunnel: Theory, design and construction* (pp. 267–274). London: Taylor & Francis Group.

Liu, X., & Yuan, D. (2015). Mechanical analysis of anti-buoyancy safety for a shield tunnel under water in sands. *Tunnelling and Underground Space Technology, 47*, 153–161.

Mo, H. H., & Chen, J. S. (2008). Study on inner force and dislocation of segments caused by shield machine attitude. *Tunnelling and Underground Space Technology, 23*, 281–291.

Ruan, W. J. (2005). Spreading model of grouting in rock mass fissures based on time-dependent behavior of viscosity of cement-based grouts. *Chinese Journal of Rock Mechanics and Engineering, 24*, 2709–2714.

Talmon, A. M., & Bezuijen, A. (2009). Simulating the consolidation of TBM grout at Noordplaspolder. *Tunnelling and Underground Space Technology, 24*, 493–499.

Talmon, A. M., & Bezuijen, A. (2013). Analytical model for the beam action of a tunnel lining during construction. *International Journal for Numerical and Analytical Methods in Geomechanics, 37*, 181–200.

Tang, M. X., Chen, R. G., & Chen, W. (2009). Stress monitoring and internal force analysis of Guangzhou metro shield tunnel segment during construction. *China Civil Engineering Journal, 42*, 118–124.

Ye, F., Chen, Z., & Jia, T. (2016). Penetration diffusion model of exponential fluid for backfill grouting through segments of shield tunnel. *China Journal of Geotechnical Engineering, 38*, 890–897.

Youn, B., & Breitenbücher, R. (2014). Influencing parameters of the grout mix on the properties of annular gap grouts in mechanized tunneling. *Tunnelling and Underground Space Technology, 43*, 290–299.

Zhang, S. S., Dai, Z. R., & Bai, Y. (2012). Research on dissipation law of grout pressure during the simultaneous grouting of shield tunnel. *China Railway Science, 33*, 40–48.